Physical and Mechanical Properties of Alkali-Slag Pervious Concrete

Xu Liang[1], Kai Fang[1], Jun Huang[1,2,3,4,*], Denis Rodrigue[5], Qingxiang Zhao[1] and Chengpeng Zou[1]

[1]*College of Civil Engineering and Architecture, Wenzhou University, Wenzhou, China*

[2]*Key Laboratory of Engineering and Technology for Soft Soil Foundation and Tideland Reclamation of Zhejiang Province, Wenzhou, China*

[3]*Wenzhou Engineering Technical Research Center on Building Energy Conservation and Emission Reduction & Disaster Prevention and Mitigation, Wenzhou, Zhejiang, China*

[4]*Zhejiang Collaborative Innovation Center of Tideland Reclamation and Ecological Protection, Wenzhou, Zhejiang, China*

[5]*Department of Chemical Engineering, Laval University, Quebec, Canada*

Abstract: Alkali-activated pervious concrete was prepared using ground granulated blast furnace slag (GGBS) as a cementitious material substitute and sodium silicate as an alkali activator. This study investigated the effects of water-binder ratio, sodium silicate modulus, and alkali equivalent on the mechanical properties, permeability coefficient, and chloride ion resistance of the pervious concrete. The results showed that as the water-binder ratio increased from 0.27 to 0.31, the mechanical properties improved slightly, but the permeability coefficient decreased. The optimal mechanical performance was achieved at an alkali equivalent of 6%, while the highest porosity was observed at 0.3%. A sodium silicate modulus of 1.2 provided the best balance between mechanical strength and permeability. Then, regression analysis was used to confirm a linear correlation between porosity and permeability coefficient, while the Boltzmann model was used to establish a relationship between chloride ion content and penetration depth. Finally, a comparison with previous experimental results showed that GGBS contributed to improve the mechanical properties of pervious concrete.

Keywords: Alkali activated material, Ground granulated blast furnace slag, Pervious concrete, Durability, Regression analysis.

1. INTRODUCTION

Global economic growth has intensified urban challenges like flooding, heat islands, and climate change [1]. Cement production exacerbates this: 1 ton of Portland cement emits 0.82 tons of CO_2, consuming 6.6 MJ of energy [4, 5]. Pervious concrete, a porous pavement material, offers a solution by enhancing rainwater infiltration - a core feature of sponge city construction. Ordinary Portland pervious concrete mitigates urban flooding and heat islandst [6], but suffers from low strength, clogging, and durability issues [7]. Its production exacerbates greenhouse gas (GHG) emissions and resource depletion [8] -the construction industry ranks as the second-largest GHG emitter [9], consuming 25% of global freshwater, 40% of energy, and 30% of raw materials, while generating 25% of solid waste [10]. Global construction projects drive rising concrete demand—Burj Khalifa alone used 330,000 m³ [11]. As sustainability grows crucial, cement remains dominant, making alternatives to Portland cement essential for improving permeable concrete performance and reducing reliance on traditional binders.

Alkali-activated concrete gains attention for matching/exceeding ordinary concrete's strength and durability without Portland cement [12]. Made from aluminosilicate-rich byproducts (slag, fly ash, silica fume) or natural resources (metakaolin and red mud), it's activated by alkali solutions (NaOH, Na_2SiO_3, KOH, and $NaCO_3$). With lower CO_2 emissions and similar performance, it's a promising cement alternative [13-16]. It reduces cement dependence and enables industrial waste recycling (*e.g.*, fly ash, GGBS). Scholars use these byproducts to partially replace cement, boosting resource utilization and concrete strength [17, 18]. Alkali-activated materials outperform ordinary concrete in mechanical properties, durability, and sustainability [19-21]. Research on slag (320 million tons/year [22]) as a precursor for low-carbon concrete has shown promise, despite limited current use.

Slag has higher calcium content than other alkali-activated precursors (*e.g.*, fly ash, metakaolin), accelerating early hydration product formation. Its silicon dioxide and alumina precursors enhance strength through poly-condensation [23, 24]. The high

*Address correspondence to this author at the College of Civil Engineering and Architecture, Wenzhou University, Wenzhou, China;
Tel: +86-13587607056;
E-mail: junhd@wzu.edu.cn

Received on 22-07-2025 Accepted on 29-08-2025 Published on 04-09-2025

E-ISSN: 2819-828X/25

MgO content promotes hydrotalcite ($Mg_6Al_2(OH)_{16}CO_3$) formation, boosting early strength in alkali-activated slag concrete (AASC). Thus, AASC outperforms other alkali-activated concretes in mechanical properties, temperature resistance, and chemical corrosion resistance. Additionally, its fast setting and high early strength reduce molding times, increase prefabricated component production efficiency, and lower costs [25, 26]. At the same time, slag powder particles are finer than cement particles, Hu *et al*. [27] found, by means of mercury porosimetry (MIP) and X-ray tomography (X-CT), that when the D50 of slag powder decreases from 22 μm to 11μm, the total porosity of AASC decreases from 18.7% to 12.3%, and the connected porosity decreases by more than 40%. The finer slag particles fill the gaps between cement hydration products through the “micro-filling effect”, and promote the secondary hydration reaction to generate additional gel products, making the slurry structure more denser. The filling effect of cement particles (D50=25μm) and slag powder was compared, proving that slag powder was better in refining pores and reducing permeability. For example, Shi *et al*. [28] conducted compressive strength tests on S95 slag-based concrete samples under carbonation conditions, evaluating three alkali activators—sodium hydroxide (SH), a calcium oxide/sodium carbonate combination (COSC), and a calcium hydroxide/sodium sulfate combination (CHSS)—at alkali equivalents of 4%, 6%, and 8%, with testing intervals at 3, 7, 28, 56, and 84 days. The results showed that regardless of the type of activator, the compressive strength of the concrete specimens gradually decreased. In contrast, the mechanical properties of concrete under different carbonation cycles were optimal when calcium hydroxide was used as the alkali activator. Wang *et al*. [29] used GGBS and municipal solid waste incineration bottom ash as precursors, with sodium hydroxide and water glass as alkali activators, to investigate the effects of alkali equivalent of 5.5%, 6.5%, 7.5% and 8.5% and polypropylene (PP) fiber lengths on the mechanical properties of alkali-activated concrete. The results showed that as the alkali equivalent increased, both the compressive strength and flexural strength first increased, then decreased, and finally, in the case of flexural strength, increased again. When alkali equivalent is 6.5% and PP fiber length is 15 mm, the compressive strength of alkali-activated concrete is the highest, reaching about 54.5 MPa. When alkali equivalent is 6.5% or 8.5% and PP fiber length is 12 mm, the flexural strength of alkali-activated concrete is the highest, reaching about 7.8 MPa. Chia Jung *et al*. [30] used sustainable sourced waste water glass sand as an alkali activator and a carbon-free aggregate such as recycled aggregate from construction waste to study the mechanical behavior of alkali-slag mortar. The results showed that when alkali equivalent was 3-6%, its compressive strength was 16% higher than that of traditional Portland cement mortar. An alkali equivalent of 3% increased the compressive strength of AASM by 14.8%, but for higher alkali equivalent (4-6%), the compressive strength was significantly increased (36-39%).

Industrial waste residues serve as precursors with activators to enhance concrete strength and produce pervious concrete. Typically, pervious concrete has 15-25% porosity, 0.1-0.6 cm/s permeability, and 2-10 MPa compressive strength [31]. It’s mainly used for base layers in leisure areas, parking lots, and sidewalks [34]. Zhao *et al*. [36] found that fly ash reduced early strength but increased long-term strength (56–90 days) by 10-23% in pervious concrete. Municipal solid waste incineration bottom ash (BA) [37] improved properties at densities <2.25 g/cm³ but reduced permeability and strength at higher densities. Sherfenaz *et al*. [38] demonstrated that induction furnace slag (IFS) as coarse aggregate achieved compressive strengths of 4.8-10.9 MPa (single-sized) and 9.0-22.5 MPa (dense-graded), meeting ACI standards [35] while reducing CO_2 emissions by 10.9%. He *et al*. [39] optimized pervious planting concrete at a water-binder ratio of 0.28 and 0.8% PVAP, yielding strengths of 14.2 MPa (10-20 mm gravel) and 12.8 MPa (5-10 mm gravel) with permeability coefficients of 14.96 mm/s and 9.96 mm/s, respectively.

This study aims to investigate the mechanical properties and water permeability of alkali-activated pervious concrete using varied formulations. Sodium silicate and sodium hydroxide are used to prepare alkali activators with different moduli, optimizing alkali equivalent and sodium silicate modulus. Fixing porosity at 18%, five water-binder ratios (0.22-0.31) and five alkali equivalents (3%-7%) with four sodium silicate moduli (1.0-1.6) are tested. Regression models then predict permeability performance for the tested formulations.

2. MATERIALS AND METHODS

2.1. Materials

As an important component of alkali-slag permeable concrete, slag plays a major role on the mechanical properties of permeable concrete. The slag used in this experiment is S95 granulated blast furnace slag powder produced by Henan Yuanheng Environmental Protection Engineering Co., Ltd (China). The main properties are reported in Table **1**. The sodium silicate is an industrial grade produced by Zhengzhou City Xinghe Dry Materials Co., Ltd. (China), and its basic performances are presented in Table **2**. Sodium hydroxide is pure alkali flake produced by Yihua Chemical Co., Ltd. (China), with a purity ≥99%. The

Table 1: Technical Parameters of GGBS

Parameter	Activity index (%)	Fluidity ratio (%)	Water content (%)	Density (g/cm^3)	Specific surface area (m^2/kg)
Technical standard	7d 28d	≥95	≤1.0	≥2.80	v≥400
	≥75 ≥95				
Testing result	90 99	96	0.2	2.84	472

Table 2: Technical Parameters of Sodium Silicate

mNa_2O (%)	$mSiO_2$ (%)	Modulus	Baume Degree (Be)	Water Content (%)	Density (g/cm^3)
12.27	30.8	2.59	50	50	1.46

Note: ◦ Be represents the Baume of the water glass solution, m denotes mesopores, emphasizing the porous structure characteristics of the material.

Table 3: Technical Parameters of the Coarse Aggregate

Grain size (mm)	Performance density (kg/m^3)	Bulk density (kg/m^3)	Water absorption (%)	Packing porosity (%)
5~10	1700	2832	1.1	40

coarse aggregate is basalt gravel produced by Qinyuan Landscaping Engineering Co., Ltd. of Gongyi City (China), and the gravel performance test was conducted according to GB/T14685-2011. This experiment uses a single particle size (5-10 mm), Wash with tap water and dry in an oven for 24 hours. Table **3** presents the specific parameters obtained. Wenzhou local tap water was used for all the experiments. Images of the relevant raw materials are shown in Figure **1**.

2.2. Formulation

In this study, the sodium silicate solution with alkali equivalent of 5%, water-binder ratio of 0.22, 0.25, 0.27, 0.29, 0.31, design porosity of 18% and modulus of sodium silicate of 1.2 was selected to prepare alkali slag pervious concrete. The film thickness of the paste, compressive strength, flexural strength and water permeability coefficient of the slurry were measured. In order to study the effect of alkali equivalent on mechanical properties and water permeability of alkali slag permeable concrete, alkali equivalents of 3%, 4%, 5%, 6% and 7% or sodium silicate moduli of 1.0, 1.2, 1.4, and 1.6 were selected for comparative testing, with a fixed water-binder ratio of 0.29 and designed porosity of 18%. The compressive strength, flexural strength and water permeability coefficient were measured. The mix ratio of alkali-activated slag pervious concrete is shown in Table **4**, in which S-0.22, N-1, W-1.0 denote specimens with a water-binder ratio, an alkali equivalent and a modulus of water glass of 0.22, 1 and 1.0 respectively.

2.3. Equipment and Methods

According to the real condition of alkali slag pervious concrete, a forced single horizontal shaft concrete mixer was selected for the tests. Standard cube specimens (100×100×100 mm^3) were cast for compressive strength, permeability coefficients and chloride ion penetration resistance tests, while

(a) (b) (c) (d)

Figure 1: Images of the materials used: (**a**) S95 slag; (**b**) sodium silicate solution; (**c**) NaOH; (**d**) coarse aggregate.

100×100×400 mm^3 specimens were used for flexural strength testing. All testing equipment configurations are illustrated in Figure **2**(**a**)-(**e**), including the mixer, specimen molds, and testing apparatus.

Pervious concrete exhibits relatively poor workability due to the absence of fine aggregates. On the other hand, larger inter-particle voids between coarse aggregates make the bonding strength of paste a critical factor directly influencing the concrete's mechanical properties. The performance of pervious concrete is significantly influenced by the molding method, so the selection of appropriate molding conditions is critical to produce high-quality pervious concrete. In this experiment, slag and alkali activator solution were first poured into the mixer and stirred for 60 s, followed by the addition of coarse aggregates with continued mixing for 120 s, finally the mixture is poured into molds. Compared to conventional concrete, pervious concrete exhibits a more extensive pore structure, resulting in significantly increased surface area exposure of molded specimens to air. This accelerated moisture loss consequently affects the compressive strength of pervious concrete. Therefore,

Table 4: Mix Ratio of Alkali-Activated Slag Pervious Concrete

Specimen No.	Water-binder ratio	Alkali equivalent (%)	Modulus of water glass	S95 slag (kg/m^3)	Coarse aggregate (kg/m^3)	Sodium silicate (kg/m^3)	Water (kg/m^3)
S-0.22	0.22	5	1.2	407	1543	92.31	47.33
S-0.25	0.25	5	1.2	389	1543	88.23	56.90
S-0.27	0.27	5	1.2	376	1543	85.28	62.56
S-0.29	0.29	5	1.2	363	1543	82.30	67.60
S-0.31	0.31	5	1.2	350	1543	79.40	72.21
N-3	0.29	3	1.2	376	1543	51.20	85.62
N-4	0.29	4	1.2	376	1543	68.21	77.82
N-5	0.29	5	1.2	376	1543	85.33	70.01
N-6	0.29	6	1.2	376	1543	102.34	62.23
N-7	0.29	7	1.2	376	1543	119.41	54.22
W-1.0	0.29	6	1.0	376	1543	88.78	69.57
W-1.2	0.29	6	1.2	376	1543	102.30	62.23
W-1.4	0.29	6	1.4	376	1543	112.65	56.30
W-1.6	0.29	6	1.6	376	1543	124.48	49.86

Note: In the sample codes, S represents water-binder ratio, N represents alkali equivalent, W represents water glass modulus.

(a) Concrete mixer

(b) Compression tester

(c) Universal testing machine

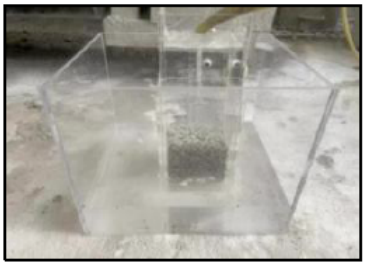

(d) Permeability coefficient equipment

(e) Shake table

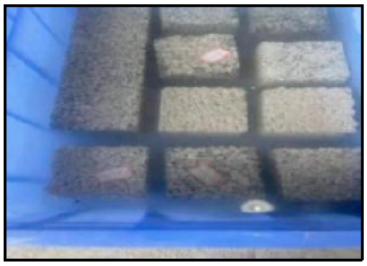

(f) Water curing

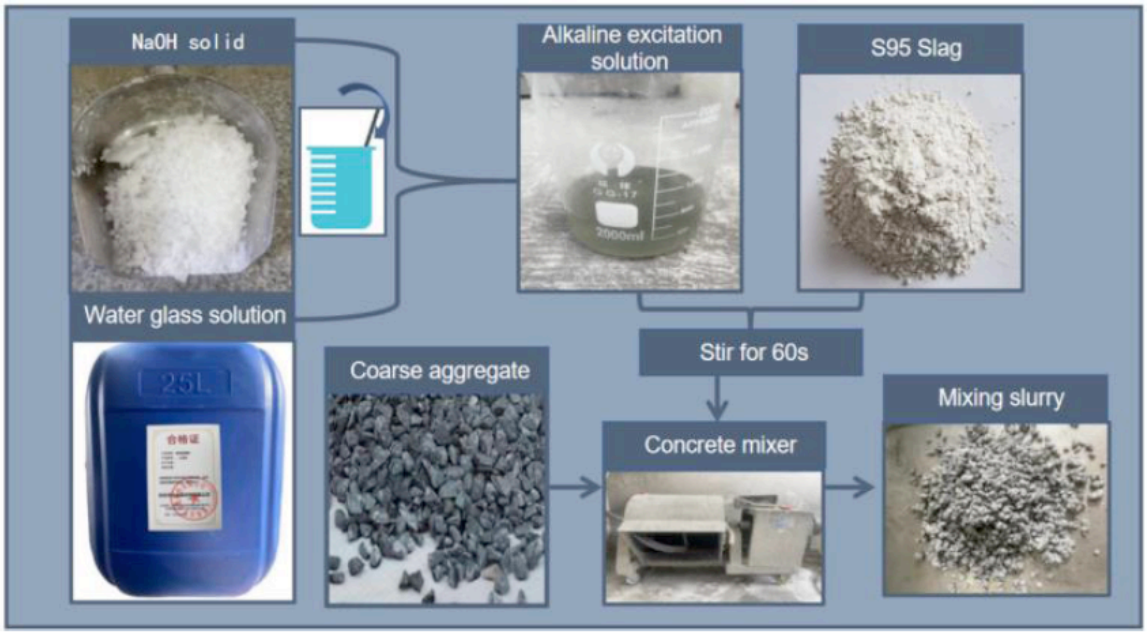

(g) Preparation flow diagram

Figure 2: Testing equipment and flow diagram.

the test specimens should be immediately covered with a plastic film after molding. The curing methods of pervious concrete mainly include natural curing, standard curing, water curing, watering film curing and hot water accelerated curing [40]. In this study, the water curing method was selected: demolding the specimens after one day and place them in water for curing. The preparation steps are shown in Figure **2** (**f**) and (**g**).

The compressive strength tests of pervious concretes were performed at a loading velocity of 8 kN/s to obtain the peak loads. Three-point flexural tests were conducted by using an universal testing machine by MTS Industrial Systems Co., Ltd (China). Displacement control was selected, and the loading rate was fixed as 0.05 mm/min. The permeability coefficient tests were conducted using the constant-head method on 100×100×100 mm^3 specimens (Figure **3a**). Porosity tests are generally done by a gravimetric method, and the corresponding equipment is shown in Figure **3b**.

After concrete pouring, the specimens underwent standard indoor curing for 28 days (20±2°C, relative humidity > 95%). They were then immersed in a 4% NaCl solution for corrosion testing over periods of 30 days or 60 days. Given the thin mortar thickness of pervious concrete after coating coarse aggregates, this experiment adopted grinding depths of 2, 4, and 6 mm. The collected powder was mixed uniformly in deionized water. After 1 day of static settling, the free chloride ion

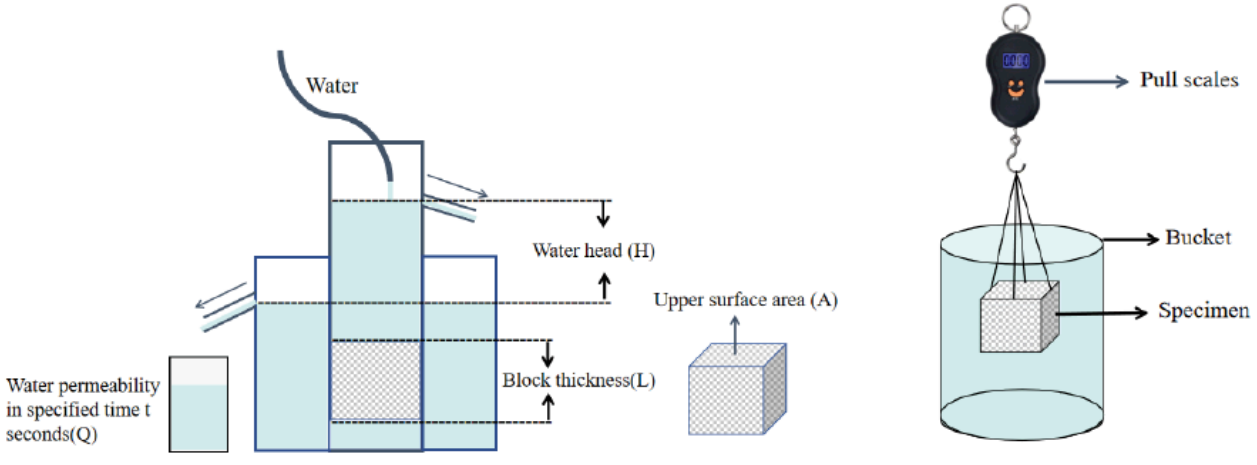

(a) (b)

Figure 3: Schematic representation of the experimental set-up used: (**a**) water permeability coefficient test device and (**b**) porosity test device.

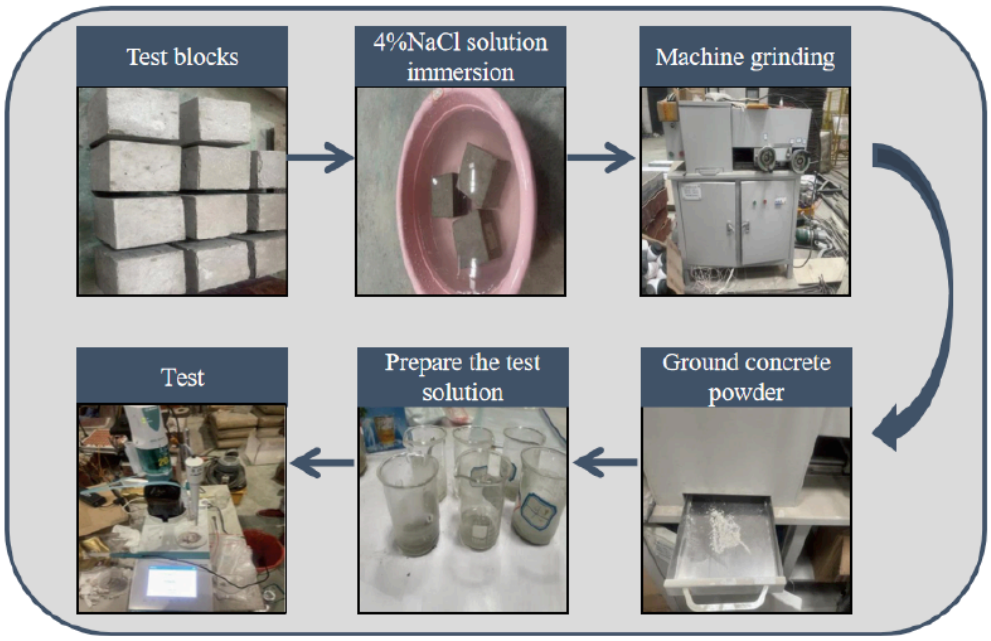

Figure 4: Steps to determine the chloride ion concentration.

concentration in the concrete samples was measured using a Swiss Metrohm 916 Ti-Touch potentiometric titrator. The corresponding process is shown in Figure **4**.

3. RESULTS AND DISCUSSION

Traditional cement-based concrete exhibits a series of drawbacks, including low tensile strength, poor wear resistance, high cost, and significant environmental pollution [41]. In contrast, alkali-activated pervious concrete prepared by substituting cement with GGBS not only reduces the environmental impact, but also generates superior mechanical properties. The porosity of pervious concrete is typically controlled within the range of 15-35% to ensure adequate permeability, with the corresponding permeability coefficient generally ranging between 0.14 and 1.22 cm/s [42-44] In this section, the mechanical properties of alkali-activated pervious concrete prepared with different water-binder ratios, alkali equivalents, and sodium silicate moduli at 7 day and 28 day of curing ages are investigated ,as well as the permeability coefficients of the specimens after complete saturation (28 day).

3.1. Mechanical Properties of Alkali Activated Pervious Concrete

3.1.1. Effects of Water-Binder Ratios

The water-binder ratio has a significant effect on the hardening process, workability, and final mechanical properties of pervious concrete [45], and the dispersion diagrams of the slurry under different water-binder ratios are shown in Figure **5**. It can be

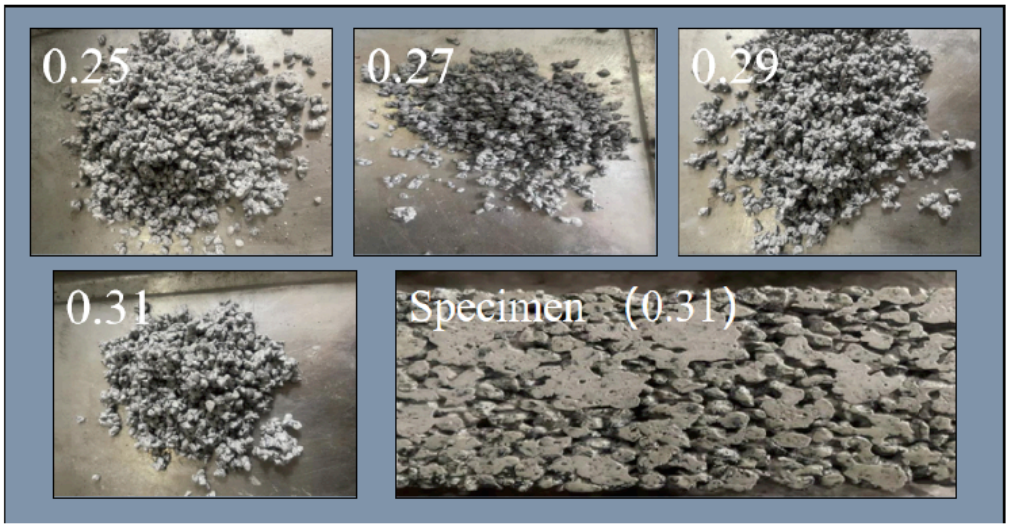

Figure 5: Mixing state diagrams of specimen with different water-binder ratios.

seen that the fresh concrete exhibited poor workability for alkali activated pervious concrete with a water-binder ratio of 0.27 was used, leading to immediate collapse of the specimen after pouring combined with the segregation of coarse aggregates. Similar issues were observed for a water-binder ratio of 0.25. Although it can be molded in a mold and maintain the shape of the mold container, loose stones were detached from the surface (or showing a lack of corners) and the compressive strength was very low when the form was removed 24 hours after casting. With a higher water-binder ratio (0.29 and 0.31), the slurry can effectively coat the aggregates, showing excellent cohesion, easy moldability, without surface aggregate spalling upon demolding. The thickness of the paste layer also significantly influenced the mechanical properties of pervious concrete [46]. It was observed that the thickness of the paste layer decreased with increasing water-binder ratio. Although thicker paste coating on coarse aggregates enhanced structural integrity and achieved higher mechanical properties, from a mixture workability and molding effectiveness point of view, a lower water-binder ratio proved detrimental to the forming of pervious concrete specimens.

Pervious concrete often has poor mechanical properties as its compressive strength typically ranges from 2.8 to 28 MPa [47] The main factors influencing the mechanical properties of pervious concrete include the size and type of aggregates, cementitious materials, water-binder ratio, aggregate-binder ratio, admixtures, and compaction methods [48, 50]. The effects of water-binder ratio are plotted in Figure **6**. The figure shows that both compressive strength and flexural strength exhibit an initial improvement with water-binder ratio increasing. Simultaneously, these mechanical properties peak at a water-binder ratio of 0.31. This phenomenon may be attributed to the optimal fluidity of the paste achieved at this ratio, enabling thorough coating of coarse aggregates. The effective bonding between aggregates through the paste enhances the overall structural integrity [51]. However, at the water-binder ratio of 0.31, partial sedimentation of the paste occurs due to gravitational effects, significantly reducing permeability. But the experimental results indicate that pervious concrete with a water-binder ratio of 0.29 exhibits higher strength than that with a ratio of 0.27. This lower strength at 0.27 ratio is attributed to inadequate paste fluidity and excessive paste film thickness around aggregates, preventing the mixture from achieving maximum compactness during mold placement. Increasing the water-binder ratio can enhance the mechanical properties of alkali-activated slag pervious concrete to some extent. Table **5** reports that the 28 day compressive and flexural strengths of this concrete exceed the 7 day values by 35% and 68% respectively, while exhibiting favorable early-age strength at a curing age of 7 days. Taking the 0.29 water-binder ratio as an example, the 7 day compressive and flexural strengths reach 85% and 70% of their 28 day counterparts respectively, with consistent strength development patterns observed across different ratios. The superior mechanical performance of alkali-slag concrete has been further validated through experimental studies by Gao *et al*. [52].

3.1.2. Effects of Alkali Equivalent

Since its initial proposal, alkali-activated concrete has garnered significant research attention, with sodium hydroxide and sodium silicate being the most commonly used activators [53-55]. The alkali equivalent denotes the mass ratio of Na_2O in alkali-activating solutions prepared from sodium hydroxide to slag mass. When the alkali equivalent ranges between 3% and 6%, both hydration heat and

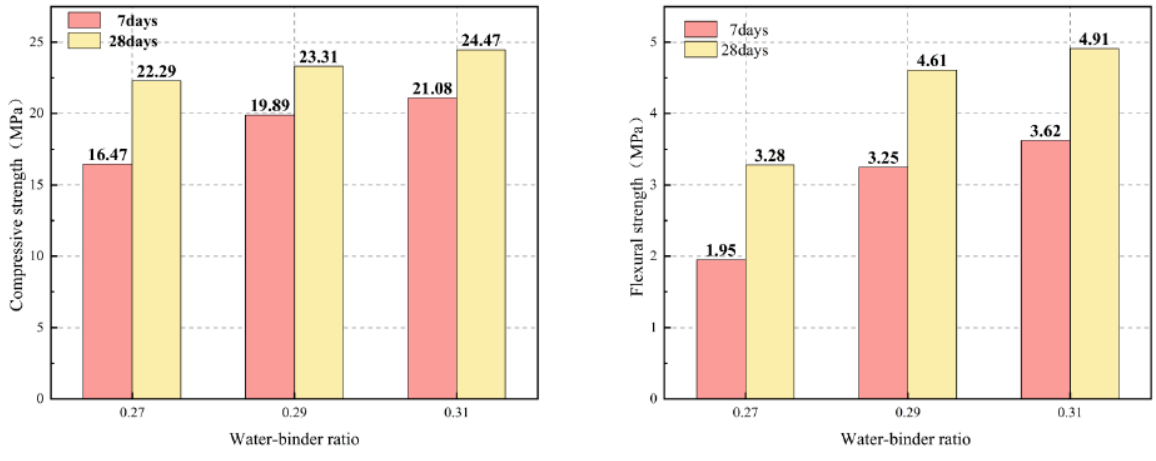

Figure 6: Effect of water-binder ratio on the mechanical properties of pervious concrete: (**a**) compressive strength and (**b**) flexural strength.

degree of hydration increase with increasing alkali content, leading to enhanced reaction kinetics where alkali addition promotes stronger molecular interactions between water and reactants, thereby improving hydration reactions. This equivalent plays a critical role in alkali-activated slag pervious concrete by governing strength development, density formation, and workability characteristics. Thus, a careful control of the alkali equivalent during mixing is essential to achieve optimal concrete performance [28].

Compressive and flexural strength tests were conducted on pervious concrete specimens with varying alkali equivalents, followed by comprehensive data analysis. As illustrated in Figure **7**, the compressive strength of alkali-activated slag pervious concrete progressively increases with higher alkali equivalents. Specimens with 3% alkali equivalent exhibit significantly lower strength than those with other equivalents due to insufficient alkali availability for complete slag reaction, resulting in incomplete condensation and hardening processes. Correspondingly, the flexural strength at this 3% equivalent is highly reduced. The mechanical strength demonstrates progressive enhancement across all specimens as the alkali equivalent increases. At 6% alkali equivalent, pervious concrete specimens show higher compressive and flexural strengths compared to 7%, reaching peak mechanical performance. This strength reduction at elevated alkali levels occurs due to excessive drying shrinkage at paste joints within the concrete matrix, inducing micro-crack formation and ultimately compromising structural integrity. Considering the above, an alkali equivalent of 6% generated optimal mechanical properties of pervious concrete. This trend aligns with other findings [53-56]. In particular, excessive alkali equivalent induces drying shrinkage within pervious concrete [57], resulting in compressive cracking during testing and ultimately reducing mechanical strength. The results of Table **5** also show that when the alkali equivalent is 3%, the compressive and flexural strength at the age of 28 days increased by 35% and 33% compared to the values at 7 days, respectively, However, when the alkali equivalent is 6%, the compressive and flexural strength of alkali-activated slag pervious concrete only increased by 15% compared to 7 days, exhibiting higher early strength.

3.1.3. Effects of Water Glass Modulus

The modulus of water glass refers to the ratio of the molar amount of SiO_2 to that of Na_2O in its solution. A higher modulus can enhance the viscosity, density, strength, and fire resistance of water glass, but reduces its solubility and ion-exchange capacity. In alkali-activated slag pervious concrete, water glass modulus critically influences mechanical properties. As depicted in Figure **8**, both compressive and flexural strengths initially rise and subsequently decline with increasing modulus. In particular, the compressive strengths for curing ages of 7 day and 28 day reach their peak values at a modulus of 1.2 (Figure **8a**). This phenomenon occurs because a lower modulus provides higher alkalinity, facilitating Ca^{2+} dissolution but inhibiting calcium silicate hydrate (C-S-H) formation. As the modulus increases, the amount of monomer $[SiO_4]^{4-}$ increases, promoting silica gel formation making the paste more compact by filling pores, thereby enhancing strength [53]. However, further modulus increase reduces the liquid-phase alkalinity, slowing slag particle dissolution and consequently decreasing the compressive strength[58]. Flexural strength follows a similar trend to compressive strength. Table **5** indicates that the compressive and flexural strengths at 7 days reach 85% of those at 28 days.

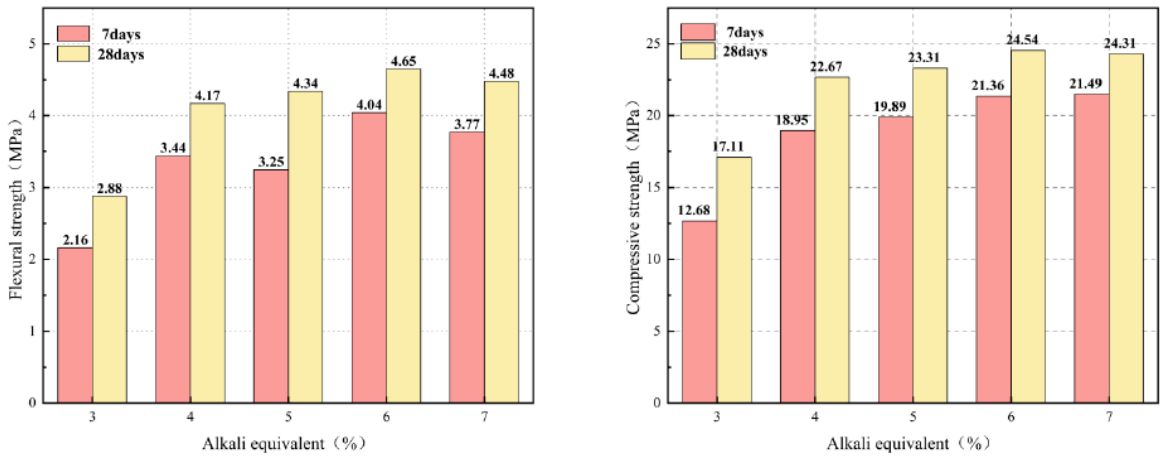

(a) (b)

Figure 7: Mechanical strength as a function of alkali equivalents: (**a**) compressive strength and (**b**) flexural strength.

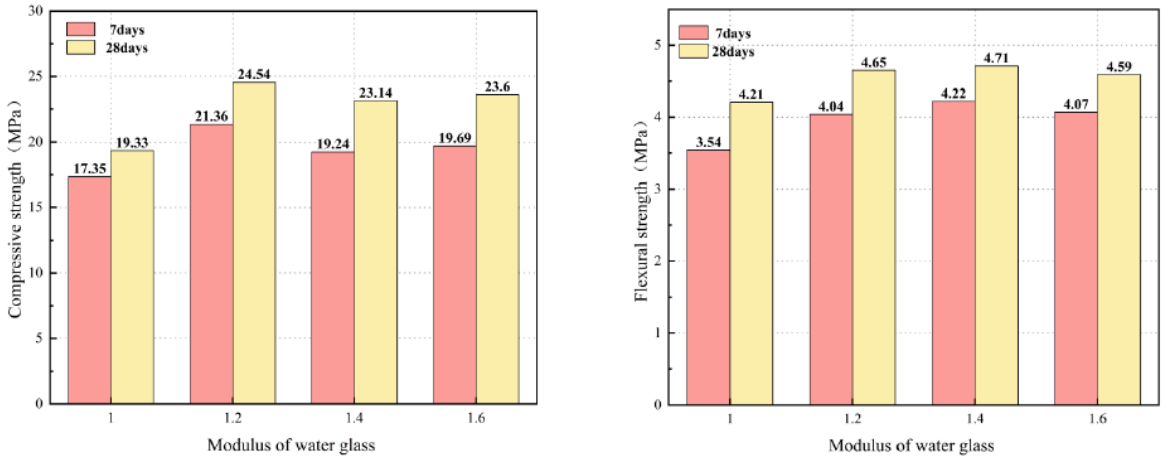

(a) (b)

Figure 8: Mechanical strength as a function of water glass modulus: (**a**) compressive strength and (**b**) flexural strength.

Table 5: Comparative Analysis of Mechanical Properties at 7 and 28 Day

Sample	Flexural Strength		Compressive Strength	
	Increasing rate	Ratios ($f_{cf,7}/f_{cf,28}$)	Increasing rate	Ratios ($f_{cc,7}/f_{cc,28}$)
S-0.27	68.2%	59.5%	35.3%	73.9%
S-0.29	41.2%	70.5%	17.2%	85.3%
S-0.31	26.1%	73.9%	16.1%	86.1%
N-3	33.3%	75.0%	34.9%	74.1%
N-4	21.2%	82.4%	19.6%	83.6%
N-5	33.5%	74.9%	17.2%	85.3%
N-6	15.1%	86.9%	14.9%	87.1%
N-7	18.8%	84.2%	13.1%	88.4%
W-1	18.9%	84.1%	11.4%	89.8%
W-1.2	15.1%	86.9%	14.9%	87.1%
W-1.4	11.6%	89.6%	20.3%	83.1%
W-1.6	12.8%	88.6%	19.9%	83.4%

3.2. Water Permeability of Pervious Concrete

3.2.1. Effects of Water-Binder Ratio

The measured porosity gradually decreases with increasing water-binder ratio, marinly because the paste exhibits poorer workability at lower water-binder ratios, preventing the concrete from achieving its densest state during pouring; the design porosity was 18%, and the measured values were slightly higher than this value. As shown in Table **6**, the permeability coefficient decreased from 18.5% to 18.1% as the water-binder ratio increased. All tested pervious concrete mixtures with varying water-binder ratios met the permeability requirement of ≥0.5 mm/s specified in the technical code CJJ/T 135-2009 "Technical Specification for Pervious Cement Concrete Pavement". However, a water-binder ratio of 0.31 experienced paste settlement during pouring, wasting some cementitious materials. It also showed a lower permeability coefficient compared to other mixtures.

3.2.2. Effect of Alkali Equivalent

Based on Table **6**, it can be observed that the permeability coefficient decreases with increasing alkali equivalent. At alkali equivalents of 3% and 4%, the measured porosities (19.5% and 18.7%) exceeded the target porosity (18%), resulting in higher permeability coefficients. When the alkali equivalent is low, insufficient alkali is available to react with the slag, leading to lower early strength, especially after one day. This caused minor dislodgement of stone particles, resulting in higher measured porosity. Conversely, at higher alkali equivalents, the increased fluidity of the alkali-activated slag paste caused the mixture to segregate during molding, with paste flowing downward. This resulted in the partial filling and blockage of some interconnected voids, reducing the

Table 6: Porosity and Permeability Coefficient of the Pervious Concrete Produced

Sample	Water-binder ratio	Alkali equivalent (%)	Modulus of water glass	Design porosity (%)	Measured porosity (%)	Permeability coefficient (mm/s)
S-0.27	0.27	5	1.2	18%	18.5	6.8
S-0.29	0.29	5	1.2	18%	18.2	5.7
S-0.31	0.31	5	1.2	18%	18.1	5.6
N-3	0.29	3	1.2	18%	19.5	6.4
N-4	0,29	4	1.2	18%	18.7	6.2
N-5	0.29	5	1.2	18%	18.2	5.7
N-6	0.29	6	1.2	18%	18.3	5.9
N-7	0.29	7	1.2	18%	17.9	5.7
W-1	0.29	6	1.0	18%	17.8	5.5
W-1.2	0.29	6	1.2	18%	18.3	5.9
W-1.4	0.29	6	1.4	18%	17.6	5.5
W-1.6	0.29	6	1.6	18%	17.2	5.2

effective porosity and consequently lowering the permeability coefficient.

3.2.3. Effects of Water Glass Modulus

As shown in Table **6**, the permeability coefficient initially increases and subsequently decreases with increasing modulus of sodium silicate, reaching its maximum value at a modulus of 1.2. At lower moduli, the higher alkalinity of the liquid phase promotes slag hydration and C-S-H formation, but adversely affects permeability. As the modulus increases, although more C-S-H forms to fill pores and enhance paste density, it simultaneously densifies the pore structure of the concrete, thereby reducing permeability. The permeability coefficient and mechanical properties of the composite material exhibit an initial rise followed by a decline as the sodium silicate modulus increases. These experimental results indicate that a sodium silicate modulus of 1.2 achieves an optimal balance between the permeability and mechanical performance of pervious concrete.

Design porosity refers to the intentional control of concrete porosity during design to meet permeability requirements. For pervious concrete, the interconnected porosity typically ranges between 15% and 25%. This metric represents the amount of interconnected voids within the concrete, enhancing its water permeability while reducing density. In this study, the target design porosity was predetermined as 18%. As indicated in Table **6**, the measured porosity values closely aligned with the design porosity. For the effect of water-binder ratio and alkali equivalent on porosity, lower water-binder ratios and lower alkali equivalents resulted in higher porosity, mainly due to reduced paste filling volume inside the concrete. This resulted in larger internal voids leading to lower mechanical performance. At a sodium silicate modulus of 1.2, the pervious concrete exhibited higher porosity and permeability. In general, the porosity for alkali-activated pervious concrete should not exceed 25%. Designers may include a porosity allowance (safety factor) to enhance the permeability coefficient without compromising mechanical properties [59].

3.3. Durability of Alkali-Slag Pervious Concrete

The volume density of pervious concrete is an important factor to control concrete quality, it can reflect the ratios of aggregate, slurry and water within the concrete and affect the durability of pervious concrete. In civil engineering, in terms of the volume density differences of pervious concrete, the unstable quality of pervious concrete caused by the raw materials fluctuations and uneven mixing can be seen. In this study, a volume density test with 6 specimens is carried out to check the quality of pervious concrete. The results are listed in Table **7** and plotted in Figure **9**. From the results, it can be seen that the average value of volume densities is 2050 kg/m^3, and the corresponding deviation is less than 0.5%.

Table 7: Volume Density of the Pervious Concrete Samples

Sample	Weight (kg)	Density kg/m^3
W1	2.05	2050
W2	2.06	2060
W3	2.05	2050
W4	2.04	2040
W5	2.04	2040
W6	2.06	2060

Note: The water-binder ratio of the specimen is 0.29, alkali equivalent is 6% and water glass modulus is 1.2.

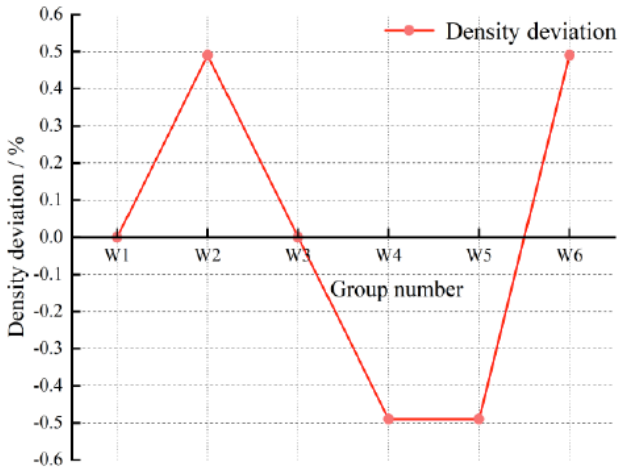

Figure 9: Density deviation of each group.

Chloride ions are characterized by high reactivity, small ionic radius, and strong permeability, and their effect on concrete durability is mainly manifested via the following aspects: chloride ions penetrating concrete reducing the pH of pore solutions, disrupting the passive film on steel reinforcement surfaces, subsequently inducing corrosion-induced expansion of steel bars leading to internal cracking [60, 61]. Inside concrete, some chloride ions exist as free ions dissolved in pore solutions, while others bind chemically or physically through reactions with hydration products [62]. Unlike conventional concrete, alkali-activated pervious concrete lacks steel reinforcement; thus, chloride-induced corrosion mainly affecting the concrete matrix itself. Owing to the diversity of aluminosilicate materials, the hydration products and pore structures of alkali-activated cementitious materials vary significantly, resulting in considerable differences in chloride penetration resistance [63]. The primary hydration products consist of calcium aluminosilicate hydrate (C-A-S-H) and sodium aluminosilicate hydrate (N-A-S-H) gels. N-A-S-H gel typically exhibits loosely structured gel pores, while C-A-S-H gel features more continuous and dense pores, providing superior resistance to chloride ion penetration [64]. By measuring chloride ion concentration at varying depths, the durability of concrete structures can be predicted, generating information for subsequent maintenance strategies. To compare chloride resistance between alkali-activated slag cementitious materials and conventional cement-based binders, chloride ion concentrations at different depths were determined in specimens immersed in NaCl solution for both cement-based concrete and alkali-activated slag concrete.

From Table **8** and Figure **10**, it is clear that regardless of whether the corrosion duration was 30 days or 60 days, chloride ion concentration decreased significantly with increasing depth. When the specimen depth reached 6 mm, the concentration approached negligible values (detection levels). Compared to plain concrete, the chloride ion concentration in alkali-activated slag concrete at equivalent depths was substantially lower due to its denser microstructure, in which chloride ions diffuse at a slower rate.

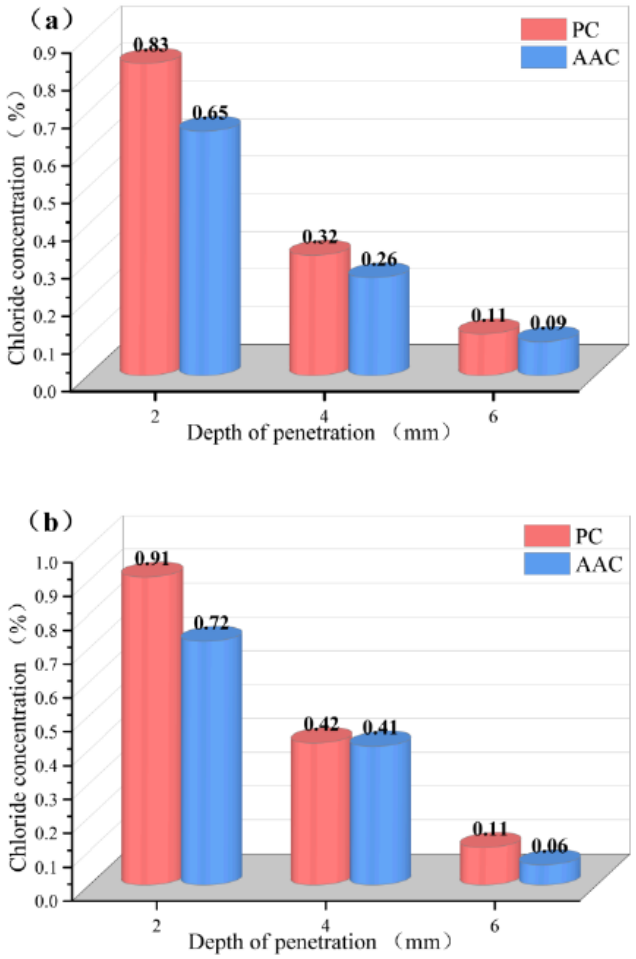

Figure 10: Chlorine ion concentration as a function of the depth of penetration at different corrosion time: (**a**) 30 days and (**b**) 60 days.

Table 8: Formulations Tested for the Chloride Ion Resistance Test

Sample	Cement kg/m^3	Water kg/m^3	Coarse aggregate kg/m^3	Fine aggregate kg/m^3	S95 slag kg/m^3	Alkali activator kg/m^3	Water-binder ratio
PC	400	180	1150	630	—	—	0.45
AAC	—	130	1080	720	400	109	0.45

Note: PC stands for plain concrete and AAC stands for alkali-activated concrete.

3.4. Regression Analysis

3.4.1. Chloride Ion Concentration and Depth of Penetration

In order to get a relationship between the chloride ion concentration and the penetration depth, regression analysis (linear fitting) was selected to analyze the experimental data of alkali activated slag concrete. The fitting results ae plotted in Figure **11**. It can be seen that the chloride ion concentration varies linearly with position whatever the corrosion duration (30 days or 60 days) as the determination coefficients are above 0.85 for both cases.

At 30 days, the coefficient of determination (R^2 = 0.90) indicates a high degree of fit, demonstrating a significant linear relationship between chloride ion concentration (y) and penetration depth (x): chloride ion concentration decreases linearly with increasing penetration depth, with an average decrease of 0.14% per 1 mm depth increment. At 60 days, R^2 further improves to 0.99, reflecting a stronger linear attenuation of chloride ion concentration with depth, where the concentration decreases by 0.165% on average for each 1 mm increase. A comparison of the two fitted lines reveals significant temporal differences in chloride ion penetration behavior. The 60-day fitted line exhibits a higher intercept (1.0567) than the 30-day line (0.8933), demonstrating that prolonged corrosion increases the initial chloride ion concentration at the concrete surface for equivalent penetration depths, which reflects continuous chloride penetration and accumulation over time. Furthermore, the absolute slope value of the 60-day line (-0.165) exceeds that of the 30-day line (-0.14), indicating accelerated chloride ion concentration decay with depth under extended exposure. This enhanced attenuation rate suggests either: (1) an intensified retardation effect of the concrete's internal structure against chloride penetration with prolonged corrosion time, or (2) altered diffusion paths caused by hydration products progressively filling pore spaces. The fitting results provide critical insights into the chloride ion penetration resistance of alkali-activated slag concrete. Both fitted lines exhibit significant linear attenuation ($R^2 \geq 0.90$), confirming that chloride diffusion follows a steady-state mechanism consistent with Fick's second law. Notably, the 60-day line demonstrates a steeper slope (-0.165 vs. -0.14 at 30 days) and higher intercept (1.0567 vs. 0.8933), revealing two synergistic phenomena: (1) enhanced surface chloride enrichment due to prolonged corrosion, and (2) increased internal resistance to penetration, evidenced by the accelerated concentration decay rate (larger absolute slope value). This suggests a time-dependent strengthening of the "gradient retardation" effect, likely attributable to either progressive pore structure refinement from ongoing hydration reactions or altered ion transport pathways. Consequently, the chloride permeability resistance of alkali-activated slag concrete improves with extended curing/corrosion duration.

3.4.2. Porosity and Permeability Coefficient

The measured fitting relationship between porosity and permeability coefficient has clear statistical significance in pervious concrete research. Multiple experiments indicate that an increase in porosity (especially effective porosity) significantly enhances the permeability coefficient, with the underlying mechanism being that the connectivity of pore channels and pore size distribution directly affect the water permeation path. When the porosity increases

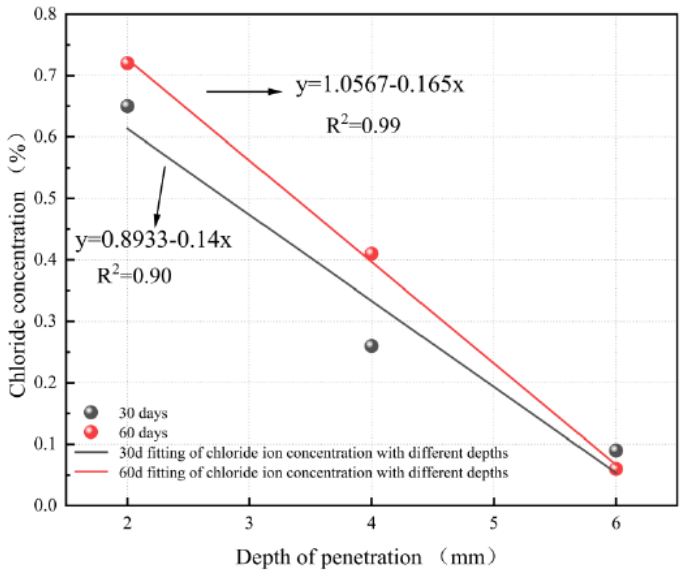

Figure 11: Linear regression for the chloride ion concentration as a function of penetration depth.

Table 9: Non Linear Fitting Parameters (Boltzmann Model)

Parameter	A_1	A_2	x_0	dx	R^2
Value	16.84	18.56	5.48	0.21	0.89
Standard error	0.60	0.10	0.16	0.10	

from 15% to 25%, the permeability coefficient can be improved by 50%-200%, which validates the theoretical basis of porosity as a core parameter for permeability performance. The Boltzmann model (equation 1) was applied to fit the correlation between porosity and permeability coefficient, with the fitting parameters listed in Table **9**. The fit is good, with a coefficient of determination (R^2) of 0.89, indicating a strong but non-linear relationship between the variables. Previous studies have shown that above a porosity threshold (20-25%) [65], the increasing rate of the permeability coefficient slows significantly (Figure **12**).

$$y = \frac{A_1 - A_2}{1+e^{(x-x_0)/dx}} + A_2 \quad (1)$$

Where, x_0, dx, A_1 and A_2 refer to center, width, initial y value and final y value. The y value at x_0 is half way between the two limiting values A_1 and A_2. The y value changes drastically within a range of x variable. The width of this range is approximately dx.

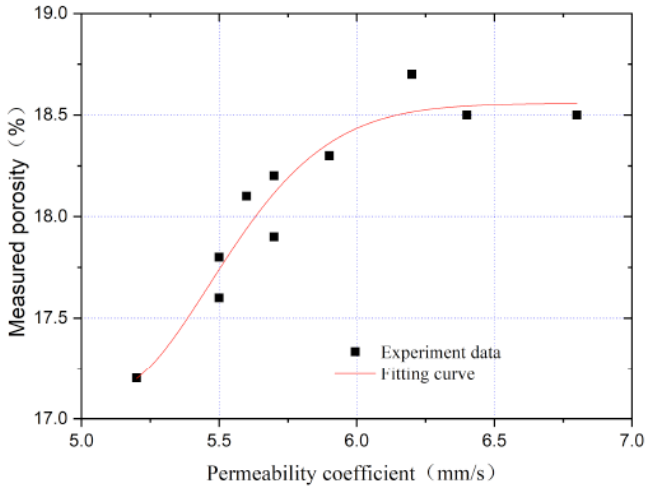

Figure 12: Fitting curve for the measured porosity as a function of the permeability coefficient.

4. DISCUSSION

4.1. Micro-Mechanism

Based on previous experiments, considering the mechanical properties and water permeability of permeable concrete, the optimum water-binder ratio is 0.29, with an alkali equivalent of 6% and a sodium silicate modulus of 1.2. To better understand the failure mechanism of pervious concrete, scanning electron microscopy (SEM) was used to analyze the surface paste and internal microstructure of the pervious concrete under this formulation. Figure **13** shows that the alkali-activated slag pervious concrete exhibits a smoother and more uniform paste surface with fewer microcracks, and the slag paste effectively coats the coarse aggregates, which helps explaining its superior mechanical performance. However, at the damaged areas in the specimen, where basalt coarse aggregates are exposed and separated from the alkali-slag paste, numerous fine cracks are present along the edges of the internal fracture zones, which may negatively impact the specimen's strength.

The alkali activation process induces a complete reaction between the activator and slag, forming cohesive and dense hydration products that interweave into a three-dimensional network, effectively filling capillary pores to create a homogeneous and smooth micro-structure. The resulting calcium silicate hydrate (C-S-H) gel from alkali-activated slag reactions demonstrates superior pore-filling capability, significantly reducing micro-crack initiation compared to conventional cement systems. This system exhibits markedly lower shrinkage during setting and hardening, with minimal deformation preventing stress-induced micro-cracking-a critical factor for mechanical strength preservation given that cracking constitutes a primary mechanism of strength degradation. The alkali-activated slag paste displays optimal rheological properties: its balanced viscosity ensures complete aggregate coating without segregation (preventing gravity-induced flow) or poor particle dispersion (avoiding excessive viscosity). This facilitates the formation of a dense interfacial transition zone where hydration products chemically bond with reactive sites on aggregate surfaces through pozzolanic reactions, significantly enhancing interfacial strength.

The mechanical failure mechanism of alkali-activated slag concrete with basalt aggregates involves three critical aspects: interfacial transition zone (ITZ) behavior, crack propagation dynamics, and stress redistribution. The significant elastic modulus mismatch (typically 60-80 GPa for basalt vs. 20-30 GPa for alkali-activated matrix) creates stress concentration factors exceeding 1.5 at ITZ regions, making these zones preferential failure initiation sites (Figure **13a**). At the same time, there may be

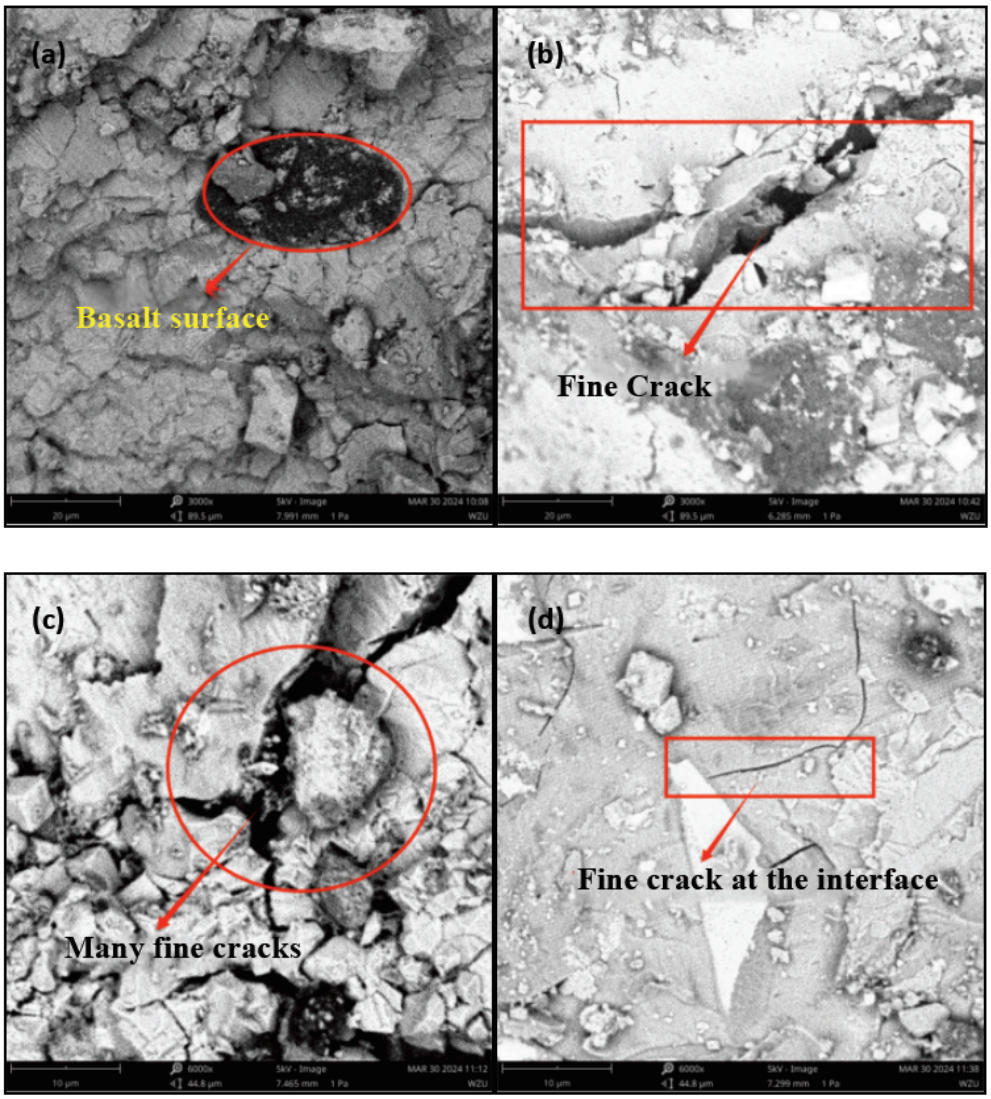

Figure 13: SEM images of failed specimen: (**a**) Basalt surface, (**b**) cracks at 3000X, (**c**) cracks at 6000X, and (**d**) the interface.

microscopic defects in the specimen itself, such as micropores and microcracks. Under external loads, these defects become crack initiation points (Figure **13b**). As the load continuously increases, cracks propagate along the path of least energy consumption. At the edge of specimen failure, cracks easily extend and propagate in multiple directions due to the complex stress state, forming more fine cracks (Figure **13c**). When the load on the specimen exceeds the bearing capacity of the alkali-activated slag slurry, the slurry itself fails. At the failure location, the slurry can no longer wrap the coarse aggregate due to its failure, leading to exposed coarse aggregate (Figure **13d**). Simultaneously, the stress release produced during slurry failure promotes the formation of new fine cracks in the surrounding area.

4.2. Comparison

Although alkali-activated pervious concrete exhibits excellent properties such as early strength and permeability, these characteristics still vary significantly depending on parameters such as cementitious materials, water glass modulus, and water-binder ratio. To investigate the influence of these parameters on the mechanical properties and permeability coefficient of pervious concrete, several representative studies were compared with the results of this study (Table **10** and Figures **14**, **15**).

Huang *et al*. [66] used water glass with a modulus of 1.3, along with metakaolin (MK) and GGBS, to prepare pervious concrete. The results showed that the compressive and flexural strengths at the age of 7 day and 28 day were 20.7 MPa, 22.8 MPa and 3.3 MPa, 3.6 MPa respectively, slightly lower than the results of this study (Figures **14**, **15**). Tan *et al*. [67] studied the effects of different water glass moduli on the mechanical properties, porosity, and permeability coefficient of alkali-activated pervious concrete by replacing slag with varying amounts of fly ash. Due to the low long-term strength of fly ash, even with a water glass modulus of 1.4, the compressive strength at the

Table 10: Comparison of the Mechanical and Physical Properties for Different Studies

Reference	Binder material	Water glass modulus	Water-binder ratio	Compressive strength 7 d/28 d MPa	Flexural strength 7 d/28 d MPa	Permeability coefficient mm/s	Porosity %
This study	S95 GGBS	1.2	0.29	21.4/25.5	4.0/4.6	3.6-6.8	17.2-19.5
[66]	Metakaolin, GGBS	1.3	0.3	20.7/22.8	3.3/3.6	4.5-10.5	16-24
[67]	Fly ash GGBS	1.4	0.35	—/22.1	—	1.8-3.6	15-26.5
[68]	Fly ash GGBS	1.6	0.4	—/37.0	—/5.75	0.32-1.57	15-25
[69]	Fly ash GGBS	1.2	0.3	—/16.8	—	0.46-1.85	10.1-21.2
[70]	S95 GGBS	1.2	0.39	34.4/48.2	7.4/12.6	0.7-3.6	14.5-28.5
[71]	Fly ash	—	0.45	11.4/—	—	19.2-59.6	28.7-34.4
[72]	Fly ash	—	—	13.6/—	—	7.1-15.6	21.7-27.4
[73]	Fly ash S95 GGBS	1	0.32	16.03/21.84	2.0/2.22	2.5-2.7	19-22.5
[74]	Metakaolin GGBS	1.5	0.38	20.3/—	—	3.0-3.2	15.4-17.4

age of 28 day was only 22.1 MPa (Figure **14b**). Gowda *et al*. [68] adopted a higher modulus of water glass of 1.6, the actual porosity of alkali-activated permeable concrete was increased by 20% compared with the cement control group, and the permeability coefficient of alkali-activated permeable concrete was better than that of the control group. The compressive strength and flexural strength of alkali-activated permeable concrete reached 37MPa and 5.75MPa respectively after 28 days, respectively (Figures **14b**, **15**). Xu *et al*. [69] prepared alkali-activated recycled aggregate pervious concrete using fly ash and GGBS as cementitious materials with a water glass modulus of 1.2. Compared with this study, their pervious concrete exhibited lower compressive strength and permeability (Table **10**).

From Figure **14** and **15**, it can be observed that Chen *et al*. [70] adjusted the water glass modulus and alkali equivalent to produce brick-mixed recycled pervious concrete with balanced mechanical properties and permeability. When the slag content was 50%, the mechanical properties of the specimens reached the maximum. Compared with this study, the performance of their pervious concrete was superior, likely due to the higher GGBS content, which formed dense hydration products, further enhancing mechanical properties.

In contrast, Tawatchai *et al*. [71] and Vanchai Sata *et al*. [72] both used fly ash as the cementitious material to prepare pervious concrete. However, when fly ash was used, the early mechanical properties of the specimens were lower, showing a significant difference compared to the alkali-activated slag-based pervious concrete in this study. A comparison with Li *et al*. [73], who studied fly ash-slag geopolymer pervious concrete, revealed that the mechanical properties were optimal when the alkali activator modulus was 1.0 and the alkali equivalent was 6%. The 28 day compressive strength of the prepared specimens reached 21.84

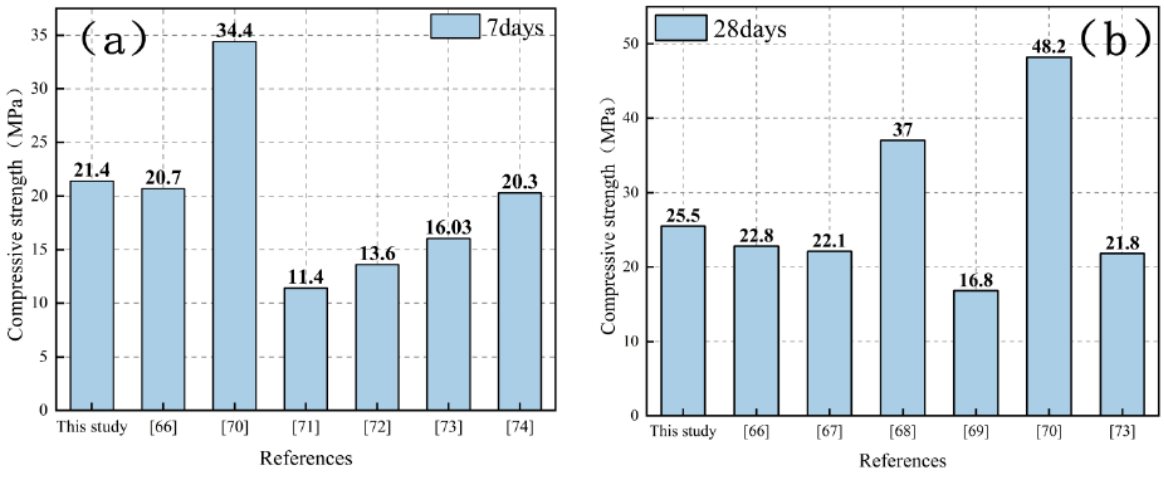

Figure 14: Comparison of the compressive strength obtained with literature result.

MPa, but the 28 day permeability ranged between 2.5–2.7 mm/s. Sun *et al.* [74] reported that using metakaolin and GGBS as cementitious materials, the compressive strength of pervious concrete could reach 20.3 MPa within 7 days, with a permeability coefficient of approximately 3.2 mm/s, which is close to the results of this study.

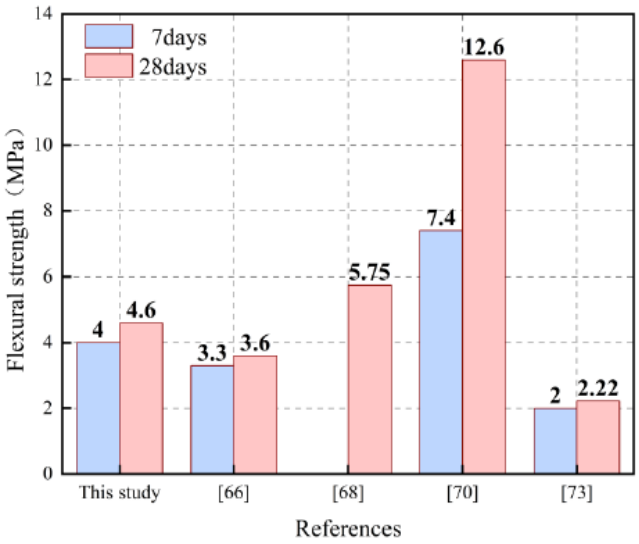

Figure 15: Comparison of the flexural strength obtained with literature results.

5. CONCLUSIONS

Alkali-activated slag pervious concrete exhibits excellent properties such as environmental friendliness and early strength due to its use of industrial waste as a cement substitute. This study conducted experiments on the effects of water-binder ratio, alkali equivalent, and sodium silicate modulus on the mechanical and permeability properties of alkali-activated slag pervious concrete, using fitting and comparative analysis methods. The main conclusions are as follows:

(1) Mechanical performance tests revealed that the optimal mechanical properties were achieved with an alkali equivalent of 6%, a water-binder ratio of 0.31, and a sodium silicate modulus of 1.2-1.4;

(2) With increasing water-binder ratio, the porosity and permeability decreased. The maximum porosity and permeability coefficient were observed at an alkali equivalent of 3%-4%, while a sodium silicate modulus of 1.2 provided the best permeability performance. Additionally, alkali-activated slag concrete showed superior resistance to chloride ion erosion compared to conventional concrete.

(3) Regression analysis indicated a linear correlation between chloride ion content and penetration depth, with determination coefficients of 0.90 (30 days) and 0.99 (60 days). The relationship between porosity and permeability coefficient followed the Boltzmann model, yielding a determination coefficient of 0.89.

(4) Comparative analysis with reported results showed that GGBS content and sodium silicate modulus enhanced the mechanical properties of pervious concrete, while fly ash and metakaolin had no significant effect, especially fly ash reduced the compressive and flexural strength of pervious concrete. When fly ash or metakaolin is added excessively, the strength of fly ash decreases due to “insufficient reaction and loose structure”, while metakaolin weakens the performance due to “excessive reaction and increased brittleness”. Finally, the mechanical properties decrease significantly by destroying the quality of gel products, pore structure and interface transition zone.

ACKNOWLEDGEMENTS

This study was supported by the National Natural Science Foundation of China (Grant Number: 51568009), Natural Science Foundation of Zhejiang Province (Grant Number: LY18E080028) and Science and Technology plan Project of Wenzhou, China (Grant Number: S20190001, S20220005).

DECLARATIONS

Conflict of Interest

We declare that we do not have any commercial or associative interest that represents a conflict of interest in connection with the work submitted.

Ethical Approval

This article does not contain any studies with human participants or animals performed by any of the authors.

REFERENCES

[1] Pierrehumbert R. There is no Plan B for dealing with the climate crisis[J]. Bulletin of the Atomic Scientists, 2019, 75(5): 215-221. https://doi.org/10.1080/00963402.2019.1654255

[2] Wang B, Wang B, Lv B, *et al*. Impact of motor vehicle exhaust on the air quality of an urban city[J]. Aerosol and Air Quality Research, 2022, 22(8): 220213. https://doi.org/10.4209/aaqr.220213

[3] Yang K, Hou H, Li Y, *et al*. Future urban waterlogging simulation based on LULC forecast model: A case study in Haining City, China[J]. Sustainable Cities and Society, 2022, 87: 104167. https://doi.org/10.1016/j.scs.2022.104167

[4] Arbi K, Nedeljkovic M, Zuo Y, *et al*. A review on the durability of alkali-activated fly ash/slag systems: advances, issues, and perspectives[J]. Industrial & Engineering Chemistry Research, 2016, 55(19): 5439-5453. https://doi.org/10.1021/acs.iecr.6b00559

[5] Xu D, Cui Y, Li H, *et al*. On the future of Chinese cement industry[J]. Cement and Concrete Research, 2015, 78: 2-13. https://doi.org/10.1016/j.cemconres.2015.06.012

[6] Zheng X, Pan J, Easa S, *et al*. Utilization of copper slag waste in alkali-activated metakaolin pervious concrete[J]. Journal of Building Engineering, 2023, 76: 107246. https://doi.org/10.1016/j.jobe.2023.107246

[7] Singh A, Sampath P V, Biligiri K P. A review of sustainable pervious concrete systems: Emphasis on clogging, material characterization, and environmental aspects[J]. Construction and Building Materials, 2020, 261: 120491. https://doi.org/10.1016/j.conbuildmat.2020.120491

[8] Kajaste R, Hurme M. Cement industry greenhouse gas emissions–management options and abatement cost[J]. Journal of cleaner production, 2016, 112: 4041-4052. https://doi.org/10.1016/j.jclepro.2015.07.055

[9] International Energy Agency (IEA), 2019. World Energy Outlook 2019 (www.eia.gov/ieo).

[10] UNEP, 2009. Buildings and climate change: Summary for decision-makers. United Nations Environ. Program. Sustain. Build. Clim. Initiat. Paris 1, 62.

[11] Subramanian N. Burj Khalifa World's Tallest Structure[J]. New Build. Mater. Constr. World, 2010, 7: 198-210.

[12] Caron R, Patel R A, Dehn F. Experimental study on basic and drying creep for an alkali-activated slag concrete and comparison with existing creep models[J]. Structural Concrete, 2023, 24(5): 6405-6420. https://doi.org/10.1002/suco.202300134

[13] Shi C, Jiménez A F, Palomo A. New cements for the 21st century: The pursuit of an alternative to Portland cement[J]. Cement and concrete research, 2011, 41(7): 750-763. https://doi.org/10.1016/j.cemconres.2011.03.016

[14] Payá J, Monzó J, Borrachero M V, *et al*. Reuse of aluminosilicate industrial waste materials in the production of alkali-activated concrete binders[M]//Handbook of alkali-activated cements, mortars and concretes. Woodhead Publishing, 2015: 487-518. https://doi.org/10.1533/9781782422884.4.487

[15] Aiken T A, Kwasny J, Sha W, *et al*. Mechanical and durability properties of alkali-activated fly ash concrete with increasing slag content[J]. Construction and Building Materials, 2021, 301: 124330. https://doi.org/10.1016/j.conbuildmat.2021.124330

[16] Pacheco-Torgal F, Castro-Gomes J, Jalali S. Alkali-activated binders: A review. Part 2. About materials and binders manufacture[J]. Construction and building materials, 2008, 22(7): 1315-1322. https://doi.org/10.1016/j.conbuildmat.2007.03.019

[17] Khan A, Do J, Kim D. Experimental optimization of high-strength self-compacting concrete based on D-optimal design[J]. Journal of Construction Engineering and Management, 2017, 143(4): 04016108. https://doi.org/10.1061/(ASCE)CO.1943-7862.0001230

[18] Ding M, Yu R, Feng Y, *et al*. Possibility and advantages of producing an ultra-high performance concrete (UHPC) with ultra-low cement content[J]. Construction and Building Materials, 2021, 273: 122023. https://doi.org/10.1016/j.conbuildmat.2020.122023

[19] Pacheco-Torgal F, Castro-Gomes J, Jalali S. Alkali-activated binders: A review: Part 1. Historical background, terminology, reaction mechanisms and hydration products[J]. Construction and building Materials, 2008, 22(7): 1305-1314. https://doi.org/10.1016/j.conbuildmat.2007.10.015

[20] Pacheco-Torgal F, Castro-Gomes J, Jalali S. Alkali-activated binders: A review. Part 2. About materials and binders manufacture[J]. Construction and building materials, 2008, 22(7): 1315-1322. https://doi.org/10.1016/j.conbuildmat.2007.03.019

[21] Pacheco-Torgal F, Abdollahnejad Z, Camões A F, *et al*. Durability of alkali-activated binders: a clear advantage over Portland cement or an unproven issue?[J]. Construction and Building Materials, 2012, 30: 400-405. https://doi.org/10.1016/j.conbuildmat.2011.12.017

[22] Miller S A, John V M, Pacca S A, *et al*. Carbon dioxide reduction potential in the global cement industry by 2050[J]. Cement and concrete research, 2018, 114: 115-124. https://doi.org/10.1016/j.cemconres.2017.08.026

[23] Garcia-Lodeiro I, Fernández-Jimenez A, Pena P, *et al*. Alkaline activation of synthetic aluminosilicate glass[J]. Ceramics International, 2014, 40(4): 5547-5558. https://doi.org/10.1016/j.ceramint.2013.10.146

[24] Provis J L. Alkali-activated materials[J]. Cement and concrete research, 2018, 114: 40-48. https://doi.org/10.1016/j.cemconres.2017.02.009

[25] Schilling P J, Roy A, Eaton H C, *et al*. Microstructure, strength, and reaction products of ground granulated blast-furnace slag activated by highly concentrated NaOH solution[J]. Journal of materials research, 1994, 9(1): 188-197. https://doi.org/10.1557/JMR.1994.0188

[26] Fang S, Lam E S S, Li B, *et al*. Effect of alkali contents, moduli and curing time on engineering properties of alkali activated slag[J]. Construction and Building Materials, 2020, 249: 118799. https://doi.org/10.1016/j.conbuildmat.2020.118799

[27] Hu X, Shi C, Shi Z, *et al*. Compressive strength, pore structure and chloride transport properties of alkali-activated slag/fly ash mortars[J]. Cement and Concrete Composites, 2019, 104: 103392. https://doi.org/10.1016/j.cemconcomp.2019.103392

[28] Shi P, Falliano D, Yang Z, *et al*. Investigation on the anti-carbonation properties of alkali-activated slag concrete: Effect of activator types and dosages[J]. Journal of Building Engineering, 2024, 91: 109552. https://doi.org/10.1016/j.jobe.2024.109552

[29] Wang C, Zhao X, Zhang X, *et al*. Effects of alkali equivalent and polypropylene fibres on performance of alkali-activated municipal waste incineration bottom ash-slag mortar[J]. Journal of Building Engineering, 2024, 84: 108496. https://doi.org/10.1016/j.jobe.2024.108496

[30] Tsai C J. Investigate the mechanical behavior of alkali-activated slag mortar using sustainable waste sodium silicate-bonded sand as an alkali activator and carbon free aggregate[J]. Construction and Building Materials, 2024, 429: 136448. https://doi.org/10.1016/j.conbuildmat.2024.136448

[31] Khankhaje E, Salim M R, Mirza J, *et al*. Properties of quiet pervious concrete containing oil palm kernel shell and cockleshell[J]. Applied Acoustics, 2017, 122: 113-120. https://doi.org/10.1016/j.apacoust.2017.02.014

[32] Rangelov M, Nassiri S, Haselbach L, *et al*. Using carbon fiber composites for reinforcing pervious concrete[J]. Construction and Building Materials, 2016, 126: 875-885. https://doi.org/10.1016/j.conbuildmat.2016.06.035

[33] Chindaprasirt P, Hatanaka S, Chareerat T, *et al*. Cement paste characteristics and porous concrete properties[J]. Construction and Building materials, 2008, 22(5): 894-901.

[34] Najm H, Wang H, Roda A M, *et al*. The use of porous concrete for sidewalks[R]. 2017. https://doi.org/10.1016/j.conbuildmat.2006.12.007

[35] ACI (American Concrete Institute). Report on pervious concrete[C]. Farmington Hills, MI, USA: American Concrete Institute, 2010.

[36] Zhao H K, Geng Q L, Liu X S. Influence of freeze–thaw cycles on mechanical properties of pervious concrete: From experimental studies to discrete element simulations[J]. Construction and Building Materials 2023, 409. https://doi.org/10.1016/j.conbuildmat.2023.133988

[37] Song H, Fan S J, Che J H, *et al*. Physical & mechanical properties of pervious concrete incorporating municipal solid waste incineration bottom ash[J]. Journal of Building Engineering 2024, 96. https://doi.org/10.1016/j.jobe.2024.110599

[38] Sherfenaz A, Ahmad S I, Salauddin M. Sustainable use of induction furnace slag as coarse aggregate in pervious concrete: Strength and hydrological properties[J]. Case Studies in Construction Materials 2025, 22. https://doi.org/10.1016/j.cscm.2025.e04653

[39] He J, Xu S H S, Sang G C *et al*. Enhancing the Mechanical Properties and Water Permeability of Pervious Planting Concrete: A Study on Additives and Plant Growth[J]. Materials (Basel) 2024, 17, (10). https://doi.org/10.3390/ma17102301

[40] Li J, Xia J, Di Sarno L, *et al*. Towards a better binder for pervious concrete: a case study on the flexural strength of fibre-reinforced high-strength cementitious paste (F-HSCP) under different curing conditions[J]. Case Studies in Construction Materials, 2025: e05059. https://doi.org/10.1016/j.cscm.2025.e05059

[41] Kanakubo T. Tensile characteristics evaluation method for ductile fiber-reinforced cementitious composites[J]. Journal of Advanced Concrete Technology, 2006, 4(1): 3-17. https://doi.org/10.3151/jact.4.3

[42] Sata V, Chindaprasirt P. Use of construction and demolition waste (CDW) for alkali-activated or geopolymer concrete[M]//Advances in construction and demolition waste recycling. Woodhead Publishing, 2020: 385-403. https://doi.org/10.1016/B978-0-12-819055-5.00019-X

[43] Elango K S, Gopi R, Saravanakumar R, *et al*. Properties of pervious concrete–A state of the art review[J]. Materials Today: Proceedings, 2021, 45: 2422-2425. https://doi.org/10.1016/j.matpr.2020.10.839

[44] Claudino G O, Rodrigues G G O, Rohden A B, *et al*. Mix design for pervious concrete based on the optimization of cement paste and granular skeleton to balance mechanical strength and permeability[J]. Construction and Building Materials, 2022, 347: 128620. https://doi.org/10.1016/j.conbuildmat.2022.128620

[45] Feng H, Su Y, Guo A, *et al*. Mechanical properties of cellulose nanocrystal modified cement/fly ash pastes under various water/binder ratios[J]. Construction and Building Materials, 2024, 447: 138213. https://doi.org/10.1016/j.conbuildmat.2024.138213

[46] Zhang Z, Pan T, Guo R, *et al*. The effect of mortar film thickness on the fluidity of concrete: Experiment and simulation[J]. Construction and Building Materials, 2024, 447: 138096. https://doi.org/10.1016/j.conbuildmat.2024.138096

[47] Tahiri I, Dangla P, Vandamme M, *et al*. Numerical investigation of salt-frost damage of pervious concrete at the scale of a few aggregates[J]. Cement and Concrete Research, 2022, 162: 106971. https://doi.org/10.1016/j.cemconres.2022.106971

[48] Adosi B, Mirjalili S A, Adresi M, *et al*. Experimental evaluation of tensile performance of aluminate cement composite reinforced with weft knitted fabrics as a function of curing temperature[J]. Polymers, 2021, 13(24): 4385. https://doi.org/10.3390/polym13244385

[49] Mardani M, Lavassani S H H, Adresi M, *et al*. Piezoresistivity and mechanical properties of self-sensing CNT cementitious nanocomposites: Optimizing the effects of CNT dispersion and surfactants[J]. Construction and Building Materials, 2022, 349: 128127. https://doi.org/10.1016/j.conbuildmat.2022.128127

[50] Supriya A, Murali K. The development of the compressive strength of pervious concrete using sugarcane bagasse ash and flyash[J]. Materials Today: Proceedings, 2023. https://doi.org/10.1016/j.matpr.2023.04.338

[51] ACI-552R, Report on Pervious Concrete, American Concrete Institute, ACI 522R-10(2010).

[52] Gao Y, Xu J, Bai E, *et al*. Static and dynamic mechanical properties of high early strength alkali activated slag concrete[J]. Ceramics International, 2015, 41(10): 12901-12909. https://doi.org/10.1016/j.ceramint.2015.06.131

[53] Yan Z, Sun Z, Yang J, *et al*. Mechanical performance and reaction mechanism of copper slag activated with sodium silicate or sodium hydroxide[J]. Construction and building materials, 2021, 266: 120900. https://doi.org/10.1016/j.conbuildmat.2020.120900

[54] Adediran A, Yliniemi J, Moukannaa S, *et al*. Enhancing the thermal stability of alkali-activated Fe-rich fayalite slag-based mortars by incorporating ladle and blast furnace slags: Physical, mechanical and structural changes[J]. Cement and Concrete Research, 2023, 166: 107098. https://doi.org/10.1016/j.cemconres.2023.107098

[55] Sun Z, Vollpracht A. Isothermal calorimetry and in-situ XRD study of the NaOH activated fly ash, metakaolin and slag[J]. Cement and Concrete Research, 2018, 103: 110-122. https://doi.org/10.1016/j.cemconres.2017.10.004

[56] Arioz O, Bzeni D K H, Zangy R R A, *et al*. Properties of slag-based geopolymer pervious concrete for ambient curing condition[C]//IOP Conference Series: Materials Science and Engineering. IOP Publishing, 2020, 737(1): 012068. https://doi.org/10.1088/1757-899X/737/1/012068

[57] Mohamed O A, Zuaiter H A, Najm O. Shrinkage characteristics of sustainable mortar and concrete with alkali-activated slag and fly ash Binders: A focused review[J]. Materials Today: Proceedings, 2024. https://doi.org/10.1016/j.matpr.2024.05.058

[58] Tan Y, He Y, Cui X, *et al*. The influence of different water glass moduli on the chemical corrosion resistance of alkali-activated porous concrete[J]. Construction and Building Materials, 2024, 415: 134971. https://doi.org/10.1016/j.conbuildmat.2024.134971

[59] Hasan M R, Zain M F M, Hamid R, *et al*. A comprehensive study on sustainable photocatalytic pervious concrete for storm water pollution mitigation: a review[J]. Materials Today: Proceedings, 2017, 4(9): 9773-9776. https://doi.org/10.1016/j.matpr.2017.06.265

[60] Zhao R D, Yang S Y, Jia W T, *et al*. Review of recent progress in durability of fly ash based geopolymer concrete[J]. J. Southwest Jiaotong Univ, 2021, 56: 1065-1074.

[61] Masoule M S T, Bahrami N, Karimzadeh M, *et al*. Lightweight geopolymer concrete: A critical review on the feasibility, mixture design, durability properties, and microstructure[J]. Ceramics International, 2022, 48(8): 10347-10371. https://doi.org/10.1016/j.ceramint.2022.01.298

[62] Wang A, Zheng Y, Zhang Z, *et al*. The durability of alkali-activated materials in comparison with ordinary Portland cements and concretes: a review[J]. Engineering, 2020, 6(6): 695-706. https://doi.org/10.1016/j.eng.2019.08.019

[63] Zhang J, Ma Y, Hu J, *et al*. Review on chloride transport in alkali-activated materials: Role of precursors, activators and admixtures[J]. Construction and Building Materials, 2022, 328: 127081. https://doi.org/10.1016/j.conbuildmat.2022.127081

[64] Osio-Norgaard J, Gevaudan J P, Srubar III W V. A review of chloride transport in alkali-activated cement paste, mortar, and concrete[J]. Construction and Building Materials, 2018, 186: 191-206. https://doi.org/10.1016/j.conbuildmat.2018.07.119

[65] Akkaya A, Çağatay İ H. Investigation of the density, porosity, and permeability properties of pervious concrete with different methods[J]. Construction and Building Materials, 2021, 294: 123539. https://doi.org/10.1016/j.conbuildmat.2021.123539

[66] Huang W, Wang H. Multi-aspect engineering properties and sustainability impacts of geopolymer pervious concrete[J]. Composites Part B: Engineering, 2022, 242: 110035. https://doi.org/10.1016/j.compositesb.2022.110035

[67] Tan Y, He Y, Cui X, *et al*. Design and performance optimization of alkali-activated waste coal bottom ash/slag porous concrete[J]. Construction and Building Materials, 2022, 359: 129413. https://doi.org/10.1016/j.conbuildmat.2022.129413

[68] Gowda S N B, Goudar S K, Thanu H P, *et al*. Performance evaluation of alkali activated slag based recycled aggregate pervious concrete[J]. Materials Today: Proceedings, 2023.

[69] Xu F, Li X, Xiong Q, *et al*. Influence of aggregate reinforcement treatment on the performance of geopolymer recycled aggregate permeable concrete: From experimental studies to PFC 3D simulations[J]. Construction and Building Materials, 2022, 354: 129222. https://doi.org/10.1016/j.conbuildmat.2022.129222

[70] Chen X, Yang Y, Zhang H, *et al*. Brick-concrete recycled aggregate/powder synergistic preparation of pervious concrete[J]. Construction and Building Materials, 2023, 407: 133517. https://doi.org/10.1016/j.conbuildmat.2023.133517

[71] Tho-In T, Sata V, Chindaprasirt P, *et al*. Pervious high-calcium fly ash geopolymer concrete[J]. Construction and Building Materials, 2012, 30: 366-371. https://doi.org/10.1016/j.conbuildmat.2011.12.028

[72] Sata V, Wongsa A, Chindaprasirt P. Properties of pervious geopolymer concrete using recycled aggregates[J]. Construction and Building Materials, 2013, 42: 33-39. https://doi.org/10.1016/j.conbuildmat.2012.12.046

[73] Li J, Zha W, Lv W, *et al*.Mechanical properties and sulfate resistance of basalt fiber-reinforced alkali-activated fly ash-slag-based coal gangue pervious concrete[J]. Case Studies in Construction Materials, 2024, 21: e03961. https://doi.org/10.1016/j.cscm.2024.e03961

[74] Sun Z, Lin X, Vollpracht A. Pervious concrete made of alkali activated slag and geopolymers[J]. Construction and Building Materials, 2018, 189: 797-803. https://doi.org/10.1016/j.conbuildmat.2018.09.067

https://doi.org/10.66000/2819-828X.2025.01.04